Speckle Imaging of Spin Fluctuations in a Strongly Interacting Fermi Gas

Christian Sanner, Edward J. Su, Aviv Keshet, Wujie Huang, Jonathon Gillen, Ralf Gommers, and Wolfgang Ketterle

Speckle Imaging of Spin Fluctuations in a Strongly Interacting Fermi Gas

Christian Sanner, Edward J. Su, Aviv Keshet, Wujie Huang, Jonathon Gillen, Ralf Gommers, and Wolfgang Ketterle

MIT-Harvard Center for Ultracold Atoms, Research Laboratory of Electronics,
and Department of Physics, Massachusetts Institute of Technology, Cambridge MA 02139

Spin fluctuations and density fluctuations are studied for a two-component gas of strongly interacting fermions along the BEC-BCS crossover. This is done by in-situ imaging of dispersive speckle patterns. Compressibility and magnetic susceptibility are determined from the measured fluctuations. This new sensitive method easily resolves a tenfold suppression of spin fluctuations below shot noise due to pairing, and can be applied to novel magnetic phases in optical lattices.

One frontier in the field of ultracold atoms is the realization of quantum systems with strong interactions and strong correlations. Many properties of strongly correlated systems cannot be deduced from mean density distributions. This has drawn interest toward novel ways of probing cold atoms, e.g. via RF spectroscopy [1, 2], Bragg and Raman scattering [3], interferometric methods [4, 5] and by recording density correlations [6–8]. Further insight into quantum systems is obtained by looking not only at expectation values, but also at fluctuations. Several recent studies looked at density fluctuations, either of bosons around the Mott insulator transition [9–11], or of a gas of non-interacting fermions [12, 13].

In this paper, we extend the study of fluctuations of ultracold gases in several ways. First, we introduce the technique of speckle imaging as a simple and highly sensitive method to characterize fluctuations. Second, we apply it to a two-component Fermi gas across the BEC-BCS crossover. Third, we directly measure fluctuations in the magnetization, i.e. the difference of the densities in the two different spin components, bypassing the need to measure the individual densities separately.

Our work is motivated by the prospect of realizing wide classes of spin Hamiltonians using a two-component gas of ultracold atoms in an optical lattice [14, 15]. An important thermodynamic quantity to characterize two-component systems is the spin susceptibility, which provides a clear signature of phase transitions or crossovers involving the onset of pairing or magnetic order [16–19]. At a ferromagnetic phase transition the susceptibility diverges, whereas in a transition to a paired or antiferromagnetic phase the susceptibility becomes exponentially small in the ratio of the pair binding energy (or antiferromagnetic gap) to the temperature. The fluctuation-dissipation theorem relates response functions to fluctuations, consequently the spin susceptibility can be determined by measuring the fluctuations in the relative density of the two spin components.

In our experiment we image the atom clouds using light detuned from resonance so that each atom's real polarizability, which contributes to the refractive index, is much larger than its imaginary polarizability, which contributes to absorption. Since the detunings for the two spin states are different, spin fluctuations lead to fluctuations in the local refractive index, resulting in phase shifts of the imaging light that vary randomly in space. We measure these phase shifts by imaging the resulting speckle patterns.
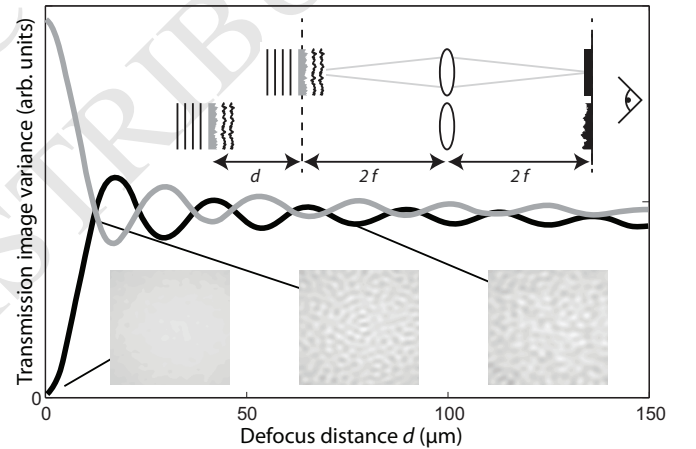

FIG. 1: Simulation of propagation effects after light has passed through a Poissonian phase noise object. Shown are the variance measured in the amplitude or in-phase quadrature (black line) and the out-of-phase quadrature (gray line) as a function of defocus distance, for an imaging system with a numerical aperture of 0.14. Within a distance less than 5 percent of our cloud size, noise becomes equally distributed between the two quadratures and the variances in transmission and phase-contrast images become the same. (Top inset) For small phase fluctuations, an in-focus phase noise object gives no amplitude contrast, but when it is out of focus it does. (Bottom inset) Sample intensity patterns for a defocused phase object.

These speckle patterns are created by propagation, which converts the spatially varying phase shifts of the imaging light into an intensity pattern on our detector without the use of a phase plate. Spin and density fluctuations occur on all spatial scales down to the interatomic separation; the smallest observable fluctuations have a

wavelength equal to the imaging system's maximum resolution. In our system that length has a Rayleigh range, and hence a depth of field, smaller then the cloud size, so the recorded image is necessarily modified by propagation effects. Propagation mixes up amplitude and phase signals (Fig. 1). This can be easily seen in the case of a phase grating, which creates an interference pattern further downstream; after propagating for a distance equal to the Rayleigh range of the grating spacing, the imprinted phase is converted into an amplitude pattern. This feature of speckle makes our imaging technique both simple and robust. It is insensitive against defocusing, and allows us to image fluctuations of the real part of the refractive index (i.e. a phase signal) without a phase plate or other Fourier optics.

Similar physics is responsible for laser speckle when a rough surface scatters light with random phases [21], and occurs when a Bose-Einstein condensate with phase fluctuations develops density fluctuations during expansion [22], or when a phase-contrast signal is turned into an amplitude signal by deliberate defocusing [23].

The experiments were performed with typically 10^6 ^{6}Li atoms in each of the two lowest hyperfine states $|1\rangle$ and $|2\rangle$ confined in an optical dipole trap oriented at $45°$ to the imaging axis with radial and axial trap frequencies $\omega_r = 2\pi \times 108.9(6)$ s^{-1} and $\omega_z = 2\pi \times 7.75(3)$ s^{-1}. For the samples imaged at 527G, the sample preparation was similar to that described in [13], with a temperature of $0.14(1)T_F$. The samples imaged at other magnetic fields were prepared in a similar fashion, except that evaporation was performed at 1000G to a final temperature of $T = 0.13(1)T_F$ before ramping the magnetic field over 1.5 s to its final value. The temperature at 1000G was determined by fitting a noninteracting Thomas-Fermi distribution in time of flight. The temperatures at other points in the crossover were related to that value assuming an isentropic ramp, using calculations presented in [24]. Using this method we obtain temperatures of $0.13(1)T_F$ at 915G, $0.19(1)T_F$ at 830G, and $0.19(3)T_F$ at 790G where additional evaporation was performed to achieve a central optical density similar to that at the other magnetic fields. The extent of the cloud along the imaging direction was 135μm, much larger than the Rayleigh range of 8μm for our imaging system with a NA of 0.14.

The superfluid to normal phase boundary was determined by measuring condensate fraction (Fig. 2) using the standard magnetic field sweep technique [25, 26]. For this, the magnetic field was rapidly switched to 570G to transfer atom pairs to more deeply bound pairs (molecules) which survive ballistic expansion. For resonant imaging of the molecules, the field was ramped back to 790G over 10 ms. The condensate fraction was determined by fitting the one-dimensional density profiles with a bimodal distribution.

As previously described, propagation converts spatial fluctuations in the refractive index into amplitude fluctu-

ations on the detector. For different choices of the probe light frequency, the two atomic spin states will have different real polarizabilities and the local refractive index will be a different linear combination of the (line-of-sight integrated) column densities n_1 and n_2. To measure the susceptibility we choose a probe light frequency exactly between the resonances for states $|1\rangle$ and $|2\rangle$, so that the real polarizabilities are opposite and the refractive index is proportional to the magnetization $(n_1 - n_2)$. The intensity fluctuations on the detector after propagation are consequently proportional to the fluctuations in magnetization. Since a refractive index proportional to $(n_1 + n_2)$ occurs only in the limit of infinite detuning, we measure the fluctuations in the total density by exploiting the fact that the fluctuations in total density can be inferred from the fluctuations in two different linear combinations of n_1 and n_2. For convenience, we obtain the second linear combination using a detuning that has the same value, but opposite sign for state $|2\rangle$, and therefore three times the value for state $|1\rangle$. With this detuning, we record images of the fluctuations in $(n_1/3 + n_2)$.
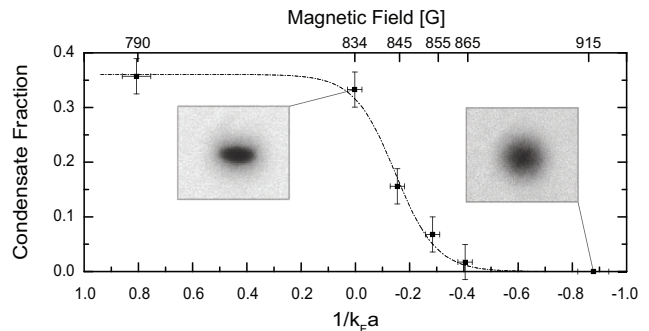

FIG. 2: Measured condensate fraction as a function of dimensionless interaction strength $1/(k_F a)$. Insets show typical images from which the condensate fraction was extracted by fitting a bimodal distribution. The dashed line is a sigmoidal fit to guide the eye.

In principle this information can be obtained by taking separate absorption images on resonance for states $|1\rangle$ and $|2\rangle$. However, the images would have to be taken on a timescale much faster than that of atomic motion and there would be increased technical noise from the subtraction of large numbers. The use of dispersive imaging has the additional advantage over absorption in that the number of scattered photons in the forward direction is enhanced by superradiance. As a result, for the same amount of heating, a larger number of signal photons can be collected [20]. This is crucial for measuring atomic noise, which requires the collection of several signal photons per atom. The choice of detuning between the transitions of the two states has the important feature that the index of refraction for an equal mixture fluctuates around zero, avoiding any lensing and other distortions of the probe beam. This is not the case for

other choices of detuning, and indeed, we observe some excess noise in those images (see below). At the detunings chosen, 10 percent residual attenuation is observed, some due to off-resonant absorption, some due to dispersive scattering of light out of the imaging system by small scale density fluctuations. The contribution to the variance of the absorption signal relative to the dispersive signal scales as $(2\Gamma)^2/\delta^2 \approx 0.006$ and can be neglected in the interpretation of the data.

The noise analysis procedure was nearly identical to that performed in [13]. A high-pass filter with a cutoff wavelength of 13μm was applied to each image of the cloud to minimize the effect of fluctuations in total atom number. Then, for each pixel position, the variance of the optical densities at that position in the different images was computed. After the subtraction of the contribution of photon shot noise, the resulting variance image reflects the noise contribution from the atoms.
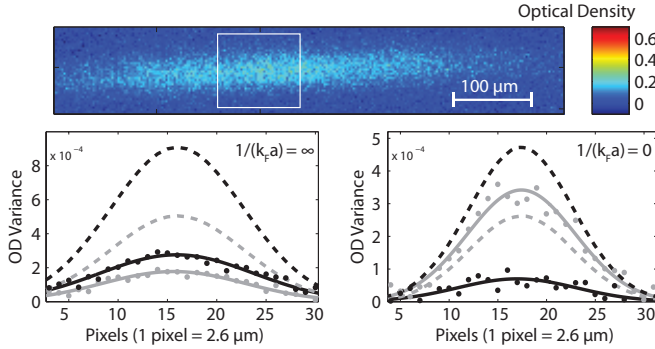

FIG. 3: (Color online) (Top) Example speckle noise image, with white box indicating analysis region. (Bottom) Noise data for noninteracting (left) and resonantly interacting (right) cold clouds, showing Δ_-^2 (black dots) and Δ_+^2 (gray dots). Solid lines are Gaussian fits to the data, and dotted lines illustrate the expected full Poissonian noise for the corresponding quantities based on density determined from off-resonant absorption.

The goal of our noise measurements is to determine at various interaction strengths the normalized susceptibility $\widetilde{\chi} = \chi/\chi_0$ and compressibility $\widetilde{\kappa} = \kappa/\kappa_0$, where $\chi_0 = 3n/2E_F$ and $\kappa_0 = 3/2nE_F$ are the susceptibility and compressibility of a zero-temperature non interacting Fermi gas with the same total density n and Fermi energy E_F. Before studying spin fluctuations through the BEC-BCS crossover, we therefore calibrate our measurement by measuring the spin fluctuations in a noninteracting mixture, realized at 527G where the scattering length between the two states vanishes. Fig. 3 shows raw profiles of the variances Δ_-^2 and Δ_+^2 measured at the two detunings. These fluctuations in the speckle pattern are proportional to number fluctuations in the specified probe volume V: $\Delta_-^2 = (c\,\Delta(N_1 - N_2))^2$ and $\Delta_+^2 = (c'\,\Delta(N_1/3 + N_2))^2$. In these relations c and c'

are factors which have to be calibrated. Without interactions, N_1 and N_2 are uncorrelated, and one predicts $(\Delta(N_1 - N_2))^2/(\Delta(N_1/3 + N_2))^2 = 2/(1 + (1/3)^2) = 1.8$. The observed ratio of $\Delta_-^2/\Delta_+^2 = 1.56(14)$ reflects excess noise contributing to Δ_+^2 due to residual systematic dispersive effects and is accounted for by setting $c'/c = \sqrt{1.8/1.56}$. For high temperatures, the atomic noise of the non-interacting gas approaches shot noise; for lower temperatures we observe a reduction in noise due to Pauli blocking as in our previous work [13]. With our new method, we easily discern spin fluctuations with a variance of less than 10 percent of atom shot noise.
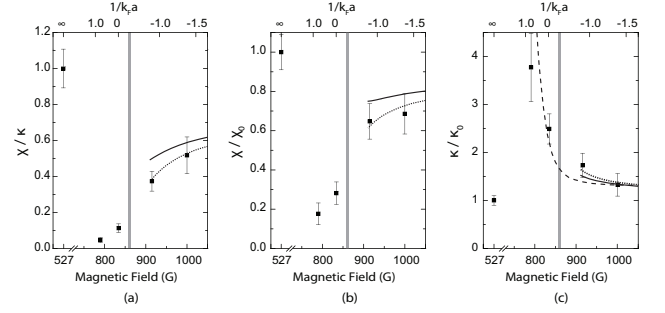

FIG. 4: (a) The ratio χ/κ, (b) the normalized susceptibility χ/χ_0, and (c) the normalized compressibility κ/κ_0 in the BEC-BCS crossover. The variances derived from sequences of images are converted into thermodynamic variables using the measured temperatures and a calibration factor determined from the noninteracting gas. The vertical line indicates the onset region of superfluidity, as determined via condensate fraction measurements. The curves show theoretical zero temperature estimates based on 1st (dotted) and 2nd order (solid) perturbative formulas obtained from Landau's Fermi-liquid theory integrated along the line of sight, and results from a Monte Carlo calculation (dashed) for the compressibility in a homogeneous system [27].

The fluctuation dissipation theorem connects the variances $(\Delta(N_1 - N_2))^2$ and $(\Delta(N_1 + N_2))^2$ to the susceptibility $\widetilde{\chi}$ and the compressibility $\widetilde{\kappa}$ via $(\Delta(N_1 - N_2))^2 = 3N/2\,(T/T_F)\,\widetilde{\chi}$ and $(\Delta(N_1 + N_2))^2 = 3N/2\,(T/T_F)\,\widetilde{\kappa}$ with $N = N_1 + N_2$ and T/T_F being the temperature measured in units of the Fermi temperature T_F. Recomposing the variances from the two experimentally accessible linear combinations these relations become $\Delta_-^2/Nc^2 = 3/2\,(T/T_F)\,\widetilde{\chi}$ and $9/4\,\Delta_+^2/Nc'^2 - 1/4\,\Delta_-^2/Nc^2 = 3/2\,(T/T_F)\,\widetilde{\kappa}$. The constants c and c' are determined using the noise measurements at 527G for a noninteracting Fermi gas for which $\widetilde{\chi} = \widetilde{\kappa} = 1 + O\left((T/T_F)^2\right)$. This analysis ignores line-of-sight integration corrections.

Fig. 4 shows the spin susceptibility, the compressibility, and the ratio between the two quantities for the interacting mixtures as the interaction strength is varied through the BEC-BCS crossover. The susceptibility and compressibility reproduce the expected qualitative behavior: for the sample at unitarity, where the transition tem-

perature is sufficiently high that a sizable portion of the sample is superfluid, and for the sample on the BEC side, the spin susceptibility is strongly suppressed relative to the compressibility. This reflects the fact that the atoms form bound molecules or generalized Cooper pairs; the spin susceptibility should be exponentially small in the binding energy, while the enhanced compressibility reflects the bosonic character of the molecular condensate. At 915G and 1000G, where the sample is above the superfluid critical temperature, the susceptibility is larger but still below its value for the noninteracting gas, reflecting the persistence of pair correlations even in the normal phase of the gas.

Above the Feshbach resonance, for attractive interactions, we compare our results to first and second order perturbation theory in the small parameter $k_F a$. This ignores the instability to the superfluid BCS state at exponentially small temperatures. The perturbation theory is formulated for the Landau parameters for a Fermi liquid [16, 28]. The susceptibility and compressibility are given by $\chi_0/\chi = (1 + F_0^a)m/m^*$, $\kappa_0/\kappa = (1 + F_0^s)m/m^*$, where $m^* = m(1 + F_1^s/3)$ is the effective mass, and F_l^s, F_l^a are the l-th angular momentum symmetric and antisymmetric Landau parameters, respectively. Although the experimental data are taken for relatively strong interactions outside the range of validity for a perturbative description, the predictions still capture the trends observed in the normal phase above the Feshbach resonance. This shows that more accurate measurements of the susceptibility, and a careful study of its temperature dependence, are required to reveal the presence of a possible pseudogap phase.

In our analysis we have neglected quantum fluctuations which are present even at zero temperature [16, 29]. They are related to the large-q static structure factor $S(q)$ measured in [30] and proportional to the surface of the probe volume, scaling with $N^{2/3} \log(N)$. For fluctuations of the total density, their relative contribution is roughly $N^{-1/3}/(T/T_F)$, and at most 40 percent for our experimental parameters. Attractive interactions and pairing suppress both the thermal and quantum spin fluctuations, but it is not known at what temperature quantum fluctuations become essential.

Spin susceptibilities can also be obtained from the equation of state which can be determined by analyzing the average density profiles of imbalanced mixtures [31]. Our method has the advantage of being applicable without imbalance, and requires only local thermal equilibrium. Moreover fluctuations can be compared with susceptibilities determined from the equation of state to perform absolute, model-independent thermometry for strongly interacting systems [32].

In conclusion, we have demonstrated a new technique to determine spin susceptibilities of ultracold atomic gases using speckle imaging. We have validated and calibrated this technique using an ideal Fermi gas and applied it to a strongly interacting Fermi gas in the BEC-BCS crossover. This technique is directly applicable to studying pairing and magnetic ordering of two-component gases in optical lattices.

[1] S. Gupta et al., Science **300**, 1723 (2003).
[2] C. A. Regal and D. S. Jin, Phys. Rev. Lett. **90**, 230404 (2003).
[3] J. Stenger et al., Phys. Rev. Lett. **82**, 4569 (1999).
[4] T. Kitagawa et al., arXiv:1001.4358 (2010)
[5] Z. Hadzibabic, S. Stock, B. Battelier, V. Bretin, and J. Dalibard, Phys. Rev. Lett. **93**, 180403 (2004).
[6] T. Jeltes et al., Nature **445**, 402 (2007).
[7] T. Rom et al., Nature **444**, 733 (2006).
[8] M. Greiner et al., Phys. Rev. Lett. **94**, 110401 (2005).
[9] N. Gemelke et al., Nature **460**, 995 (2009).
[10] W. S. Bakr et al., Science **329**, 547 (2010).
[11] J. F. Sherson et al., Nature **467**, 68 (2010).
[12] T. Müller et al., Phys. Rev. Lett. **105**, 040401 (2010).
[13] C. Sanner et al., Phys. Rev. Lett. **105**, 040402 (2010).
[14] L.-M. Duan, E. Demler, and M. D. Lukin, Phys. Rev. Lett. **91**, 090402 (2003).
[15] A. B. Kuklov and B. V. Svistunov, Phys. Rev. Lett. **90**, 100401 (2003).
[16] A. Recati and S. Stringari, arXiv:1007.4504 (2010)
[17] G. M. Bruun et al., Phys. Rev. Lett. **102**, 030401 (2009).
[18] N. Trivedi and M. Randeria, Phys. Rev. Lett. **75**, 312 (1995).
[19] C.-C. Chien and K. Levin, Phys. Rev. A **82**, 013603 (2010).
[20] W. Ketterle, D. S. Durfee and D. M. Stamper-Kurn, Making, probing and understanding Bose-Einstein condensates, in *Proceedings of the International School of Physics Enrico Fermi*, Varenna, 1998, (IOS, Amsterdam, 1999).
[21] J. W. Goodman, *Speckle Phenomena in Optics*, Ben Roberts and Company, Greenwood Village, CO, 2007.
[22] D. Hellweg et al., Phys. Rev. Lett. **91**, 010406 (2003).
[23] L. D. Turner et al., Opt. Lett. **29**, 232 (2004).
[24] Q. Chen et al., Phys. Rev. Lett. **95**, 260405 (2005).
[25] M. Greiner et al., Nature **426**, 537 (2003).
[26] M. W. Zwierlein et al., Phys. Rev. Lett. **91**, 250401 (2003).
[27] G. E. Astrakharchik, J. Boronat, J. Casulleras, and S. Giorgini, arXiv:cond-mat/0406113v1 (2004)
[28] E. Lifshitz and L. Pitaevskii, *Statistical Physics Part 2*, (Pergamon Press Inc., NY, 1980), L.D. Landau and E.M. Lifshitz, Course of Theoretical Physics, Vol. 9.

[29] G. E. Astrakharchik, R. Combescot, and L. P. Pitaevskii, Phys. Rev. A **76**, 063616 (2007).

[30] E. D. Kuhnle et al., Phys. Rev. Lett. **105**, 070402 (2010).

[31] C. Salomon, private communication

[32] D. McKay and B. DeMarco, arXiv:1010.0198 (2010)